



# Decay pathway and high-temperature luminescence of $\text{Eu}^{3+}$ in $\text{Ca}_2\text{Gd}_8\text{Si}_6\text{O}_{26}$

M.D. Chambers<sup>\*</sup>, P.A. Rousseve, D.R. Clarke

Engineering Materials Department, College of Engineering, University of California, Santa Barbara, CA 93106-5050, USA

## ARTICLE INFO

### Article history:

Received 11 June 2008

Received in revised form

3 October 2008

Accepted 13 October 2008

Available online 5 November 2008

### PACS:

32.50.+d

78.20.-e

78.55.-m

### Keywords:

Luminescence thermometry

Decay pathway

Europium phosphor

Thermal quenching

Charge-transfer state

Apatite

## ABSTRACT

The temperature-dependent luminescence of  $\text{Eu}:\text{Ca}_2\text{Gd}_8\text{Si}_6\text{O}_{26}$  and its decay pathways are investigated in order to assess the utility of the material as a thermometric phosphor. Non-radiative decays are found to compete with radiative processes even at room temperature. A decay pathway involving decay through charge-transfer states is proposed based on the decay profiles of emissions from  $^5\text{D}_1$  and  $^5\text{D}_0$  levels and on the temperature sensitivity of the spectra as observed after excitation by several wavelengths. The implications of this on solid-state lighting are also discussed.

© 2008 Elsevier B.V. All rights reserved.

## 1. Introduction

Apatite phosphors of the form  $\text{Ca}_2\text{Gd}_8\text{Si}_6\text{O}_{26}$ , activated by rare-earth ions, are often bright and highly efficient at room temperature due to the low symmetry of the sites occupied by the rare earth [1,2]. Consequently, the solid-state lighting industry has investigated their potential for down-conversion of light from UV-emitting diodes as a component of white LEDs [3]. Their high thermal stability also makes them attractive candidates for luminescence thermometry (as described elsewhere [4]). In addition,  $\text{Ca}_2\text{Gd}_8\text{Si}_6\text{O}_{26}$  has low thermal conductivity and has been observed as a reaction product in certain thermal barrier systems [5,6] and a very similar material,  $\text{Ca}_2\text{Y}_8\text{Si}_6\text{O}_{26}$ , has been found in proposed environmental barrier systems [7], systems where luminescence thermometry is of interest.

We have investigated the temperature sensitivity of the luminescence of  $\text{Eu}:\text{Ca}_2\text{Gd}_8\text{Si}_6\text{O}_{26}$ .  $\text{Eu}^{3+}$  was chosen as the luminescent species for two reasons. First, it has been demonstrated to show measurable lifetimes up to temperatures of at least 1100 °C in other hosts [8,9]. The large gap between the excited, emissive level and the next highest level has been used to explain this long lifetime in some cases [8]. Whether or not the

size of this energy gap correlates directly to persistent luminescence at high temperatures, it at least restricts the probability of direct relaxation by the emission of phonons. The second reason for selecting  $\text{Eu}^{3+}$  is because its luminescence spectra are often relatively simple compared to those of other rare earths and lends itself more readily to interpretation of its spectrum and luminescence decay profiles. In particular, most or all of the luminescence usually comes from the  $^5\text{D}_0$  state, which is a single level (that is, there is no Stark splitting). This avoids the convolution of overlapping emission peaks from different levels.

## 2. Experimental details

The material was made by a reverse co-precipitation route in order to achieve homogenous mixture of all elements involved. Methanol solutions of  $\text{Ca}(\text{NO}_3)_2$ ,  $\text{Eu}(\text{NO}_3)_3$  and  $\text{Gd}(\text{NO}_3)_3$  (all 99.99% or higher), and tetraorthoethylsilicate were mixed with a nominal cation composition corresponding to  $\text{Ca}_2(\text{Gd}_{.99}\text{Eu}_{.01})_8\text{Si}_6\text{O}_{26}$ . The dopant concentration was chosen with the intention of avoiding complications in the luminescent processes associated with interaction between nearby  $\text{Eu}^{3+}$  ions. The mixed solution was added dropwise to  $\text{NH}_4\text{OH}$  while stirring to precipitate the cations as insoluble hydroxides. The pH was maintained between 10 and 12. Then the resulting precipitate was collected by vacuum filtration, dried and calcined at 900 °C. The resulting oxide was

<sup>\*</sup> Corresponding author. Tel.: +1805 893 8138; fax: +1805 893 3882.

E-mail address: [chambers@engineering.ucsb.edu](mailto:chambers@engineering.ucsb.edu) (M.D. Chambers).

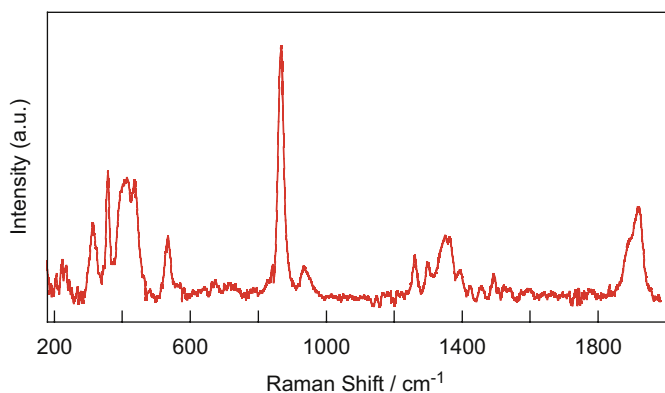


Fig. 1. Raman spectrum of the prepared polycrystalline material, indicating that the material is single-phase  $\text{Ca}_2\text{Gd}_8\text{Si}_6\text{O}_{26}$ .

crushed and ground by hand into a fine powder, pressed into a green body using polyvinyl alcohol as a binder, and finally fired and sintered at  $1200^\circ\text{C}$  for 3 h. The crystal structure of the resulting material was verified by X-ray diffraction and Raman spectroscopy (Fig. 1). No extraneous phases were detected by either technique.

Luminescence measurements were made on sintered pellets. Excitation and emission spectra were first measured with a Perkin-Elmer LS 55 spectrometer. A high-resolution Jobin-Yvon Raman microscope (T64000), using an argon ion laser tuned to 488 nm, was used to compare the emission spectrum at liquid nitrogen temperature and room temperature, as well as to measure the Raman spectrum. High-temperature measurements of spectra and decays were made with the sample inside a furnace by optical ports in the walls. Excitation was at 532 or 266 nm (doubled and quadrupled Nd:YAG, respectively) and the emitted light was collected by a silica rod extending into the furnace to a standoff of approximately 2 cm from the sample. The silica rod was coupled to a fiber optic outside the furnace and the collected light was passed through an edge filter (Semrock LP01-532RS-25 and LP01-355RU-25) to remove the laser line before being sent to a spectrometer (Ocean Optics USB2000). A variable monochromator (Acton SpectraPro 2150i) coupled to a photomultiplier tube (Hamamatsu R928, rise-time of 2.2 ns) was used to measure the signal at various wavelengths. Decays were recorded as a function of time using an oscilloscope (Lecroy WaveSurfer 62XS). Decays and spectra were recorded up to a temperature at which they could no longer be measured due to thermal quenching of the luminescence.

### 3. Observations

#### 3.1. Spectral features

Fig. 2 shows room-temperature excitation and emission spectra from  $\text{Eu}:\text{Ca}_2\text{Gd}_8\text{Si}_6\text{O}_{26}$  with the transitions labeled according to work by Liu and Chen [10] and Blasse [11]. Excitation in the ultra-violet is due to absorption into a charge transfer state (CTS) centered at approximately 260 nm and absorption into the band-gap below about 220 nm, corresponding to the temporary transfer of an electron from a coordinating oxygen to the  $\text{Eu}^{3+}$ . The emission peaks at 579 and 586 nm are of particular note. They are attributed to the  $^5\text{D}_0 \rightarrow ^7\text{F}_0$  transition. Since Stark splitting is not possible of either  $^5\text{D}_0$  or  $^7\text{F}_0$  the presence of two peaks must be due to separate emissions from the two sites occupied by the  $\text{Eu}^{3+}$  ion [3]. The  $^5\text{D}_0 \rightarrow ^7\text{F}_0$  transition is forbidden both as a magnetic dipole and an electronic dipole and it is often very weak or

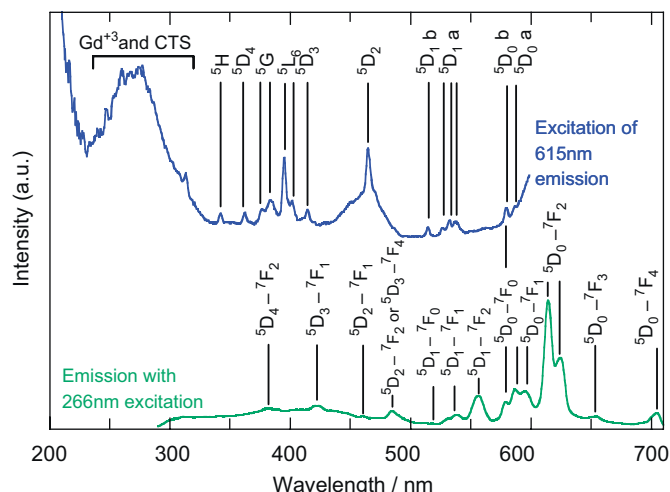


Fig. 2. Excitation and emission spectra for  $\text{Eu}:\text{Ca}_2\text{Gd}_8\text{Si}_6\text{O}_{26}$ . 266 nm excitation is absorbed into a CTS. Peak labels for levels involving transitions higher than  $^5\text{D}_1$  are tentative. The duplicity of the  $^5\text{D}_0$  level in the excitation spectrum is caused by the occupancy of two sites by  $\text{Eu}^{3+}$ .

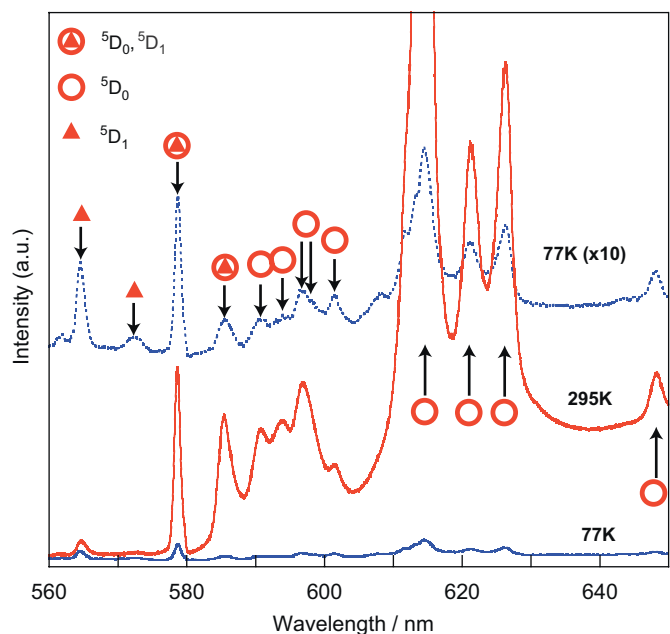
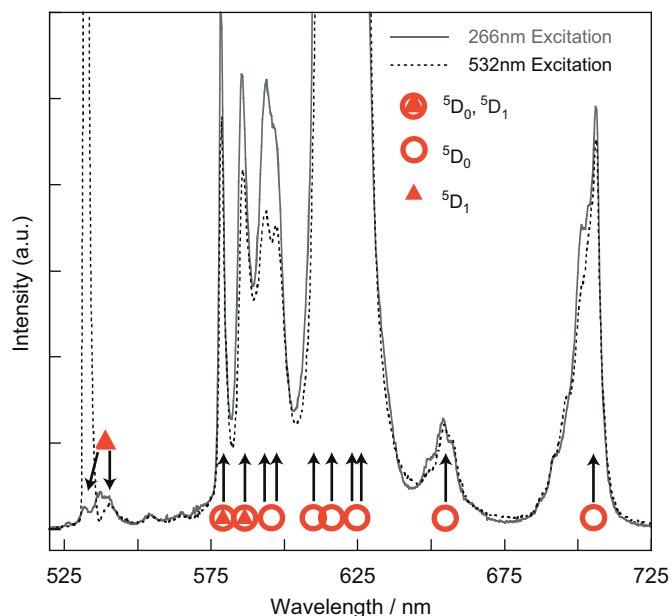


Fig. 3. Spectra at room and liquid nitrogen temperatures. For clarity the liquid nitrogen temperature spectrum is also expanded.

altogether absent, but both sites in this crystal have low symmetry ( $C_s$  and  $C_3$  for the 7-fold and 9-fold coordinate sites, respectively, Wyckoff notations  $6h$  and  $4f$ ) which relaxes the selection rules [11].

The emission spectrum was also measured after cooling to liquid nitrogen temperature with the intention of sharpening the peaks and resolving more of the peak structure. The liquid nitrogen temperature spectrum is shown in Fig. 3 in comparison to a room-temperature spectrum taken under similar conditions. The relative intensities are considered to be at least semi-quantitative. Additional peaks are resolved in the  $^5\text{D}_0 \rightarrow ^7\text{F}_1$  and  $^5\text{D}_0 \rightarrow ^7\text{F}_2$  multiplets, bringing the number of peaks to five (the maximum predicted by Blasse [11]) and at least six, respectively, if overlapping emissions from higher  $^5\text{D}$  levels can be excluded, though they cannot be with complete certainty. This suggests a



**Fig. 4.** Emission spectra after excitation with 532 and 266 nm pulsed lasers. The large peak at 532 nm for its excitation is the residual laser energy after filtering. The vertical scale has been adjusted in order to visualize the weaker  ${}^5D_1$  emissions.

strong contribution to overall luminescence from  $\text{Eu}^{3+}$  ions on both sites. Interestingly, the overall intensity of all the emission lines originating from  ${}^5D_0$  decreased dramatically upon cooling whereas the intensity of the transition from  ${}^5D_1 \rightarrow {}^7F_2$ , to which the peak at 564 nm and its satellite at 562 nm are attributed (unambiguously, as will be shown later), does not decrease significantly. The intensity of the peak at 579 nm also retains more of its strength than the other  ${}^5D_0$  lines, suggesting that it is overlapped by another line from  ${}^5D_1$ .

Spectra recorded with 266 and 532 nm pulsed laser excitation were similar to each other, as shown in Fig. 4, and similar to that observed using continuous-wave 488 nm excitation.

### 3.2. Decay features

Room-temperature lifetimes for the major peaks are tabulated in Table 1. Decays of peaks assigned to  ${}^5D_1$  had a characteristic lifetime of about 10.2  $\mu\text{s}$ , and peaks assigned to  ${}^5D_0$  had a lifetime of 1.52 ms. Note that 532 nm excites the  ${}^5D_1$  level and thus we do not have to consider transitions from higher levels. Most of the emission peaks showed decay profiles that were single exponential (e.g. the 614 nm decay in Fig. 5). The peak at 579 nm, however, shows a double-exponential decay. This is attributed to the overlap of a  ${}^5D_1$  line (the fast decay) and a  ${}^5D_0$  line (the slow decay). The peak at 586 nm also shows a double-exponential decay, indicating again a contribution from a  ${}^5D_1$  emission though the presence of this overlap is not as obvious from Fig. 3.

Filling phenomena were also observed at short times in emissions that must be ascribed solely to transitions from the  ${}^5D_0$  level. Examples of three kinds of decay—those that represent the  ${}^5D_0$  population only, those that represent the  ${}^5D_1$  population only and those that represent a mixture of both due to overlap of emission lines—are shown in Fig. 5. Over a long time-scale, the emissions at 586 nm (an overlap of  ${}^5D_1$  and  ${}^5D_0$  emissions) and 614 nm ( ${}^5D_0$  only) appear similar. On a shorter time-scale the fast part of the 586 nm decay is seen to match the 537 nm decay ( ${}^5D_1$  only), and the 614 nm decay shows an initial increase in intensity over the same region where the decay of 586 nm is fast. The functions that represent these three scenarios were used to fit the

**Table 1**  
Luminescence lifetimes of  $\text{Eu:Ca}_2\text{Gd}_8\text{Si}_6\text{O}_{26}$  after 266 nm excitation.

Lifetimes ( $\mu\text{s}$ )			
Emission (nm)	Fast decay	Slow decay	Levels
532	10.24		${}^5D_1$
537	10.27		${}^5D_1$
554	9.751		${}^5D_1$
579	10.18	1546	${}^5D_1/{}^5D_0$
586		1553	${}^5D_1/{}^5D_0$
594		1561	${}^5D_0$
597		1511	${}^5D_0$
606		1523	${}^5D_0$
614		1523	${}^5D_0$
622		1511	${}^5D_0$
626		1525	${}^5D_0$
654		1547	${}^5D_0$
706		1522	${}^5D_0$

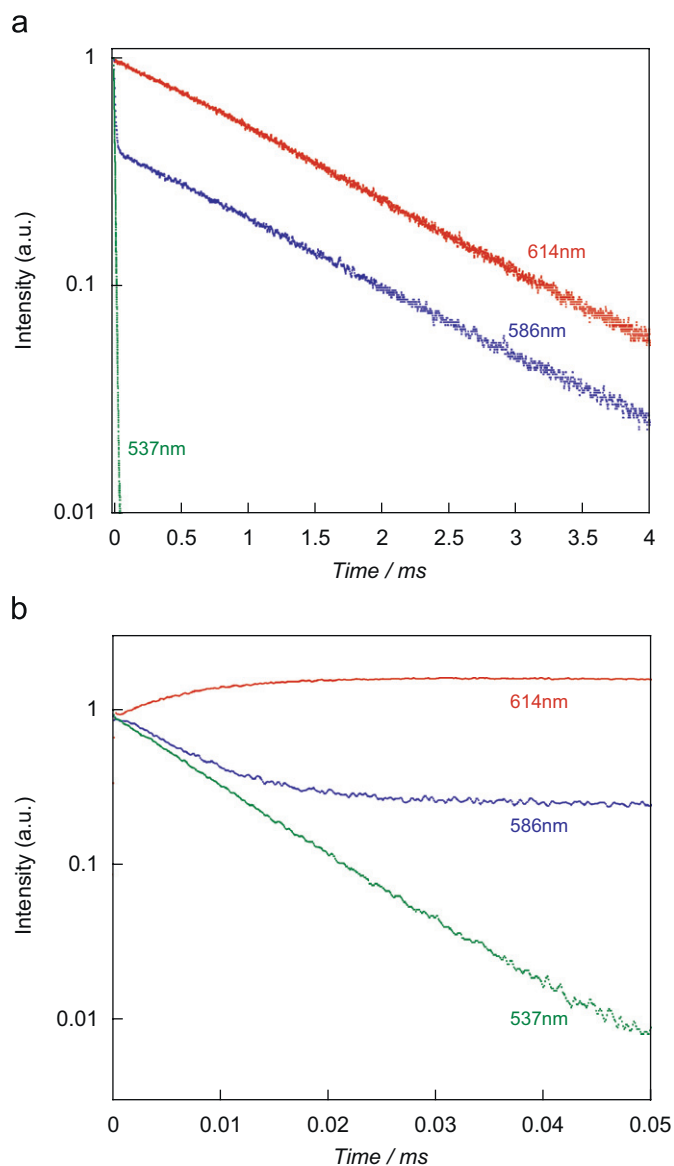


**Fig. 5.** Decays at 22  $^{\circ}\text{C}$  after pulsed excitation at 266 nm shown on two different timescales. Shown are examples of luminescence from  ${}^5D_0$  only (614 nm), luminescence from  ${}^5D_1$  only (537 nm), and mixed  ${}^5D_0$  and  ${}^5D_1$  luminescence (586 nm).

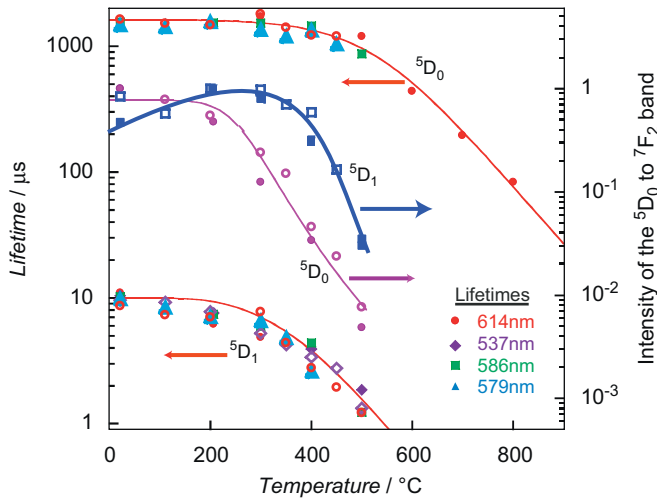


**Fig. 6.** Lifetimes measured after 266 nm excitation (closed symbols) and 532 nm excitation (open symbols), and intensity as a fraction of room-temperature intensity for both  $^5D_0$  emissions and  $^5D_1$  emissions. All fitted lifetimes, including rise-times of the 614 nm line, can be attributed unambiguously to the lifetime of either the  $^5D_0$  population or the  $^5D_1$  population. The curves through the lifetimes and the  $^5D_0$  intensities are based on Eqs 7 and 8, respectively; the curve through the  $^5D_1$  intensities is simply a best-fit line.

decay profiles are

$$I = I_0 \exp\left(\frac{-t}{\tau_1}\right) \quad 537 \text{ nm decay} \quad (1)$$

$$I = I_1 \exp\left(\frac{-t}{\tau_1}\right) + I_2 \exp\left(\frac{-t}{\tau_2}\right) \quad 586 \text{ nm decay} \quad (2)$$

$$I = \left(I_0 \left[1 - \exp\left(\frac{-t}{\tau_{rise}}\right)\right] + I'_0\right) \exp\left(\frac{-t}{\tau_2}\right) \quad 586 \text{ nm decay} \quad (3)$$

Eq. (3) describes an emission that increases in intensity for some period of time before decreasing again. It represents an exponential rise toward a maximum offset by some initial intensity (to account for some amount of direct filling), matched with a competing exponential decay towards zero. The lifetimes,  $\tau_1$  and  $\tau_2$ , represent the populations of the  $^5D_1$  and  $^5D_0$  populations respectively and the value of  $\tau_{rise}$  is found to be very close to that of  $\tau_1$ . The lifetime and rise-time data collected at various temperatures is plotted in Fig. 6. In the figure, the fitted lifetimes of lines at 614, 579, 586 and 537 nm, the fitted rise-time of the 614 nm line and the integrated intensity of the  $^5D_0 \rightarrow ^7F_2$  and  $^5D_1 \rightarrow ^7F_3$  emissions, as a fraction of room-temperature intensity, are shown as a function of temperature.

## 4. Discussion

### 4.1. Lifetimes

The measured lifetimes (Table 1) were nearly identical for all spectral lines originating from the same upper level at room temperature, and they remained quite similar at all temperatures for which they were measured (Fig. 6). The only exception was the lifetime of  $^5D_1$  as measured at 579 nm, which is slightly faster than at other wavelengths and suggests that the lifetimes of all  $^5D_1$  levels may not be exactly equal. Among the  $^5D_0$  peaks the variation is less than 2%, which is due to fitting imprecisions caused by slight non-exponential behavior in the decays. That is, Eqs. (1)–(3) do not exactly describe the decay

profiles at the long-time end. The lifetimes and rise-times, as shown in Fig. 6, can all be grouped into values representing either the  $^5D_0$  level or the  $^5D_1$  level and at all temperatures the rise-time of  $^5D_0$  is equal, within the scatter, to the lifetime of  $^5D_1$ . It is therefore concluded that the rise-time observed for  $^5D_0$  is from filling by relaxation from  $^5D_1$  (also, see note in Appendix).

Theoretically, the instantaneous intensity of the spontaneous emission of a given transition depends only on the instantaneous population of the upper level and the strength of that transition (i.e. the relevant Einstein coefficient, which is time-invariant). Therefore, the lifetime of all emissions originating from the same level of the same population of ions is identical. That lifetime, excluding any events that repopulate the upper level, is equal to the lifetime of the excited-state population—that is, it is equal to the inverse sum of the rate,  $W$ , of all de-excitation pathways, luminescent and non-luminescent alike, regardless of their nature. For example

$$\tau_{^5D_0 \rightarrow ^7F_2} = \tau_{^5D_0} = \left[ \sum_{j=0}^6 W_{^5D_0 \rightarrow ^7F_j} + \sum W_{non-radiative} \right]^{-1} \quad (4)$$

In  $\text{Eu:Ca}_2\text{Gd}_8\text{Si}_6\text{O}_{26}$  there are two major populations of  $\text{Eu}^{3+}$  ions (excluding a small number of defect-associated  $\text{Eu}^{3+}$  ions and  $\text{Eu}^{3+}$  ion pairs): those sitting on the 7-fold sites (75% of all  $\text{Eu}^{3+}$  ions) and those on the 9-fold sites (the remaining 25%). The similarity in lifetimes of all  $^5D_0$  lines is seemingly due to an intrinsic similarity in the lifetimes of these two populations. This is evidenced by the similarity of the two  $^5D_0 \rightarrow ^7F_0$  lifetimes whose peaks are sufficiently separated for measurements to be made without convolution of one lifetime with the other. Additionally, this implies that the lifetimes of  $^5D_0$ -only emission peaks are truly single exponential (except for the initial rise-time) and that deconvolution of contributions from multiple sites is unnecessary.

The possibility of energy transfer between ions must, of course, be addressed since, if fast enough, would cause all sites to appear to have the same lifetime even if the transition rates from each were different. It can also cause rise effects if the dominant emitting site is not the dominant absorbing site, as such observed in  $\text{Y}_2\text{O}_3$  doped with 3.4 mol%  $\text{Eu}^{3+}$  [12]. Site-to-site transfer can be ruled out as the cause of the rise effect seen here since the rise-time is much faster than either  $^5D_0$  lifetime. It is difficult to be certain that homogenization does not cause the similarity in  $^5D_0$  lifetimes.

A calculation was carried out to determine the average distance between  $\text{Eu}^{3+}$  ions in these two materials based on random substitution of  $\text{Eu}^{3+}$  for either  $\text{Y}^{3+}$  or  $\text{Gd}^{3+}$ . Atom positions were based on those reported for yttria by Paton and Maslen [13] and those reported for  $\text{Sr}_2\text{Nd}_8\text{Si}_6\text{O}_{26}$  by Masubuchi et al. [14], which has the same crystal structure as  $\text{Ca}_2\text{Gd}_8\text{Si}_6\text{O}_{26}$ , where corrections were made for the differences in lattice constants (i.e. the values of  $\Delta x$ ,  $\Delta y$  and  $\Delta z$  appropriate to  $\text{P6}_3/\text{m}$  were taken to be proportional to those in  $\text{Sr}_2\text{Nd}_8\text{Si}_6\text{O}_{26}$ ).

The average distance between  $\text{Eu}^{3+}$  sites in 3.4% $\text{Eu:Y}_2\text{O}_3$  is found to be 0.588 nm whereas in 1% $\text{Eu:Ca}_2\text{Gd}_8\text{Si}_6\text{O}_{26}$  the average distance is much larger: 1.049 nm. Also, in the doped apatite, less than 2% of the  $\text{Eu}^{3+}$  ions have another  $\text{Eu}^{3+}$  occupying the nearest site of opposite symmetry type (i.e.  $C_s$  and  $C_3$ ), which is at approximately 0.392 nm; see Fig. 7. Less than 6% have opposite-site  $\text{Eu}^{3+}$  ions within 0.6 nm. Additionally, 24 of the 26 oxygen atoms in the apatite formula are associated silicate groups and so are unlikely to participate in any super-exchange interaction. While some degree of homogenization cannot be ruled out based on these arguments alone, it seems unlikely that site-to-site energy exchange can account for the similarity in lifetimes observed, especially at room temperature.

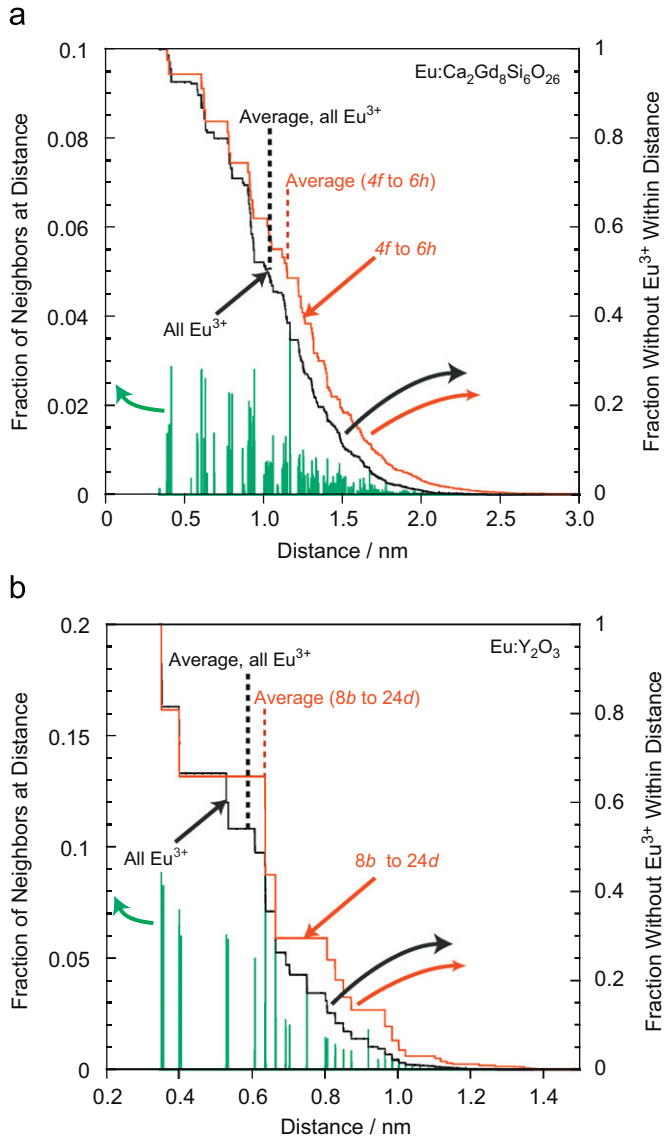


**Fig. 7.** Distributions of the distance between  $\text{Eu}^{3+}$  ions for (a)  $\text{Eu}:\text{Ca}_2\text{Gd}_8\text{Si}_6\text{O}_{26}$  (1% for  $\text{Gd}^{3+}$ ) and (b)  $\text{Eu}:\text{Y}_2\text{O}_3$  (3.4% for  $\text{Y}^{3+}$ ). The fraction of ions included with a nearest activator within a given distance is shown, and the fraction of 4f site ions included with a nearest activator on a 6h site within a given distance (or 8b to 24d for  $\text{Y}_2\text{O}_3$ ).

#### 4.2. Spectra

The change in spectrum upon cooling to 77 K (Fig. 3) suggests that the filling of  $^5\text{D}_1$ , when excited at 488 nm, is by a process that is essentially independent of temperature such as rapid filling from some metastable state (suggested by the broad peak around 480 nm in Fig. 2). But the filling of the  $^5\text{D}_0$  level depends strongly on some thermally activated process, such as phonon-assisted relaxation from  $^5\text{D}_1$  or decay from some higher level after thermal promotion to another CTS. The evidence from the decay profiles strongly supports that  $^5\text{D}_1$  fills  $^5\text{D}_0$ , and for direct excitation of  $^5\text{D}_1$  it seems reasonable that a restriction on this transition is responsible for the decrease of the  $^5\text{D}_0$  emission intensity.

As has been observed previously in  $\text{Eu}:\text{YSZ}$  and  $\text{Tb}:\text{GdAlO}_3$  [15], the rapid decrease of overall luminescence intensity with temperature (thermal quenching) begins somewhat before the measured lifetime shortens significantly.  $\text{Eu}:\text{Ca}_2\text{Gd}_8\text{Si}_6\text{O}_{26}$  is exceptionally bright at room temperature (due to the highly

non-centrosymmetric sites occupied by  $\text{Eu}^{3+}$ ) but by 500 °C it loses more than 99.5% of its intensity. The temperature of maximum emission intensity may be even somewhat above room temperature. This probably reflects an increase in losses along the filling pathway with temperature in addition to an increase in competition of non-radiative de-excitation with radiative emission, since there is insufficient change of lifetime to account for the loss of intensity according to Eq. (4).

The degree of thermal quenching observed and its early onset (at or below room temperature) has important implications for the material's use either as a phosphor for solid-state lighting or as a thermometric luminescent material. For instance, a white LED based on color mixing that uses this material for the red component will be susceptible to slight changes in color with temperature. For luminescence thermometry, both materials should also have high maximum intensity and retain good intensity at high temperature. The precision in lifetime measurements decreases as temperature increases and the signal-to-noise ratio decreases. The increase in scatter at higher temperature seen in Fig. 6 is due to this decrease in signal. Similarly, the relatively larger scatter in the  $^5\text{D}_1$  lifetimes compared to  $^5\text{D}_0$  is due to the lower intensity of those transitions. The upper bound of the utility of  $\text{Eu}:\text{Ca}_2\text{Gd}_8\text{Si}_6\text{O}_{26}$  for luminescence thermometry is ultimately set by this signal loss and is about 800 °C, depending on collection efficiency and excitation power. Temperature dependence of the decay lifetimes can be observed even at room temperature using the  $^3\text{D}_1$  emissions and the emissions from  $^5\text{D}_0$  become temperature dependent at about 500 °C. Therefore the range over which decay lifetimes from  $\text{Eu}:\text{Ca}_2\text{Gd}_8\text{Si}_6\text{O}_{26}$  could be used to measure temperature is from room temperature until about 800 °C, where the signal intensity becomes too weak to be effectively measured. It may be noted that because of this rapid thermal quenching the accidental occurrence of  $\text{Eu}:\text{Ca}_2\text{Gd}_8\text{Si}_6\text{O}_{26}$  should not cause any complications in making luminescence temperature measurements in proposed TBC or EBC systems (e.g. one based on  $\text{Eu}:\text{Gd}_2\text{Zr}_2\text{O}_7$  [8],  $\text{Gd}_2\text{SiO}_5$  and presumably  $\text{Y}_2\text{SiO}_5$  or  $\text{Y}_2\text{Si}_2\text{O}_7$ ).

#### 4.3. Temperature dependence of the non-radiative decay

The lifetime-temperature data can be fit according to a multi-phonon relaxation (MPR) model proposed by Riseberg and Moos [16] or a model based on a temperature-dependent pathway through a CTS argued for by Berry et al. [17]. The non-radiative rates,  $W_{MP}$  and  $W_{CT}$ , given by each model are

$$W_{MP}(T) = W_{MP}(0) \left( \frac{1}{\exp\left(\frac{h\nu}{kT}\right) - 1} + 1 \right)^{\Delta E/h\nu} \quad \text{MPR} \quad (5)$$

$$W_{CT}(T) = W_{CT}(0) T^{*-1/2} \exp(-E_a/kT^*) \quad \text{CTS} \quad (6)$$

$$T^* = (h\nu/2k) \coth(h\nu/2kT)$$

The overall lifetime for either model is described by

$$\tau(T) = W_{\text{Total}}^{-1} = [W_{\text{Radiative}} + W_{\text{Non-radiative}}(T)]^{-1} \quad (7)$$

where  $W_{CT}(0)$  and  $W_{MP}(0)$  are the rates of their respective processes at 0 K and are generally used as fitting terms, and the values  $\Delta E$  and  $E_a$  are the energy barriers to be crossed by the phonons. The inclusion of  $T^*$  is from a solution by Englman and Jortner [18] that accounts for the non-Arrhenius nature of CTS pathways. The value  $h\nu$  is equal to some phonon energy, rigorously an ensemble of available modes but often approximately equal to the highest mode available. In practice, if one allows  $h\nu$  to be fit as well as the other terms a suitable fit can be found using either Eq. (5) or Eq. (6) in combination with Eq. 7. From the practical standpoint of luminescence thermometry, both fits are sufficiently good for the  $^5\text{D}_0$  lifetimes (Fig. 6), but neither

fit accurately represents the  ${}^5D_1$  lifetimes. Nevertheless, thermometry based on  ${}^5D_1$  emissions could still be carried out with an empirical lifetime–temperature relationship based on the data in Fig. 6.

The question of which process is really occurring, MPR or CTS relaxation, can be partially answered by considering the fitting results from Eqs. (5) and (6). The MPR model requires  $\sim 18$  phonons at  $674\text{ cm}^{-1}$  to bridge the  ${}^5D_0$  to  ${}^7F_6$  energy gap and 8 phonons of  $219.8\text{ cm}^{-1}$  energy to relax  ${}^5D_1$  to  ${}^5D_0$ . The Raman spectrum of  $\text{Ca}_2\text{Gd}_8\text{Si}_6\text{O}_{26}$  (Fig. 1) shows a maximum energy mode at  $1923\text{ cm}^{-1}$  and several other modes above  $800\text{ cm}^{-1}$ . The validity of applying the MPR model here is doubtful due to the mismatch between phonon energies and the large number of phonons required. On the other hand, the fit based on CTS decay yields activation energies of  $6850\text{ cm}^{-1}$  for the  ${}^5D_0$  lifetimes and  $4132\text{ cm}^{-1}$  for  ${}^5D_1$ . These values seem reasonable and decay from  ${}^5D_0$  is attributed to a CTS route; decay from  ${}^5D_1$  may be more complex and include some contribution from MPR-based relaxation. These values will be taken for the position of the CTS parabola, as shown in Fig. 8. Others [19] have based the position of the CTS on absorption spectra and the temperature dependence of intensity according to simple thermal activation:

$$I = \frac{I_0}{1 + A \exp(-E_a/kT)} \quad (8)$$

The zero-position energy of the CTS is also assigned here according to the absorption spectrum, but the intensity behavior

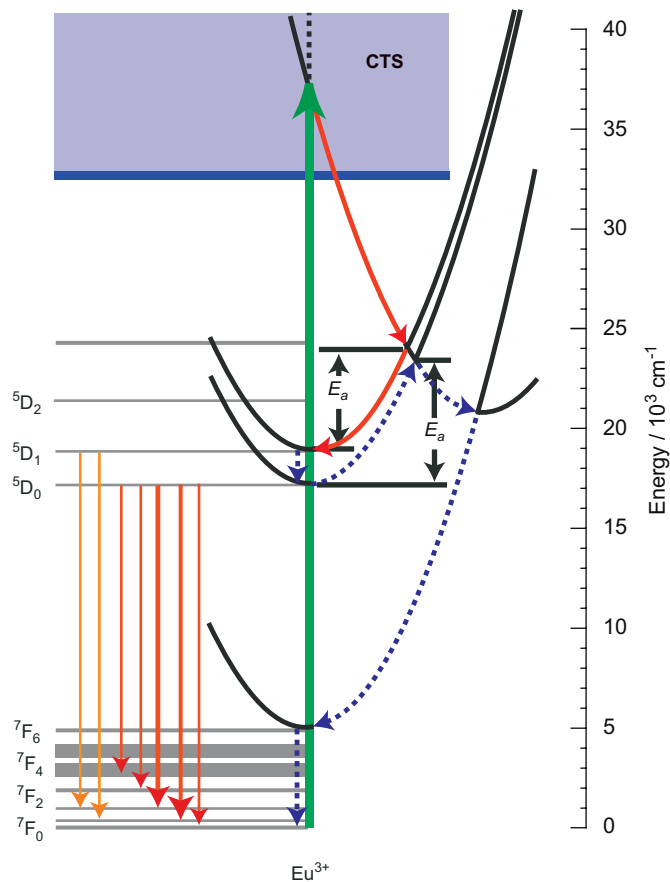


**Fig. 8.** Proposed decay pathway for  $\text{Eu}:\text{Ca}_2\text{Gd}_8\text{Si}_6\text{O}_{26}$  after UV excitation;  ${}^5D_1$  and  ${}^5D_0$  are filled from the CTS.  ${}^5D_1$  then decays both non-radiatively, to fill  ${}^5D_0$ , and radiatively. Thermally excited non-radiative decay from  ${}^5D_0$ , through a CTS, is also shown. The activation energies,  $E_a$ , for de-excitation of  ${}^5D_1$  and  ${}^5D_0$  through a CTS are shown.

reflects a more complex scenario than this equation allows for, in particular with respect to the  ${}^5D_1$  emissions (Fig. 6). Although the  ${}^5D_1$  lines are weaker than the  ${}^5D_0$  lines at all temperatures above  $22\text{ }^\circ\text{C}$ , they fall off less quickly with temperature and even show some increase with temperature from  $22$  to  $200\text{ }^\circ\text{C}$ , which is due to the nature of the filling of  ${}^5D_1$ .

The different high-temperature lifetimes observed from  $\text{Eu}^{3+}$  in different hosts depend on the position of the CTS (through the value of  $E_a$  in Eq. (6)) and the electron–lattice coupling (through  $W_{CT}(0)$ ), as well as the phonon modes of the host and whether or not another decay mechanism (such as MPR) is competitively efficient. Compared to  $\text{Eu}:\text{YSZ}$  [9] and  $\text{Eu}:\text{Y}_2\text{SiO}_5$  [22], the CTS is closer to the  ${}^5D_0$  level—that is,  $E_a$  is lower—and the value of  $W_{CT}(0)$  is also lower, suggesting a higher degree of coupling between the  $4f$  electrons of  $\text{Eu}^{3+}$  and the lattice.

The cold quenching of  ${}^5D_0$  emission seen with  $488\text{ nm}$  excitation, shown earlier, is due to direct filling of  ${}^5D_1$  and exclusively indirect filling of  ${}^5D_0$  through  ${}^5D_1$ . But in the case of  $266\text{ nm}$  excitation, a CTS is excited which fills  ${}^5D_1$  and  ${}^5D_0$  competitively (as evidenced by the non-zero starting point of the rise of the  $614\text{ nm}$  emission, Fig. 5); an increase in thermal energy increases the competitiveness of  ${}^5D_1$  filling. That is to say, the minimum of the CTS is below its cross-over with  ${}^5D_1$ . In the case of  $532\text{ nm}$  excitation the photon energy lies between  ${}^5D_1$  and  ${}^5D_0$  (when exciting from  ${}^7F_0$ ), and filling is again competitive. But thermal population of  ${}^7F_1$  is significant even at low temperatures such that 50% of the  $\text{Eu}^{3+}$  population may be sitting at  ${}^7F_1$  at  $200\text{ }^\circ\text{C}$ , according to the equation

$$\frac{N_A}{N_B} = \frac{g_A}{g_B} \exp\left(\frac{-\Delta E}{kT}\right) \quad (9)$$

where  $N$  is the population and  $g$  the degeneracy of states  $A$  and  $B$ .

Excitation from  ${}^7F_1$  to  ${}^5D_1$  is more efficient than  ${}^7F_0$  to  ${}^5D_1$  due to the closer match in energy with the  $532\text{ nm}$  photons, which accounts for the increase in intensity with temperature in this case. Therefore, the position of the CTS is assigned according to the decay lifetimes which represent the de-excitation processes in each population more or less directly rather than the spectral intensity, which depends also on the excitation processes—strongly, in this case.

Based on all these findings, a decay pathway after excitation is proposed and shown schematically in Fig. 8. Excitation for  $266\text{ nm}$  (shown) is due to the CTS which decays rapidly to fill both  ${}^5D_1$  and  ${}^5D_0$ ; this is followed by radiative transitions from  ${}^5D_1$  and  ${}^5D_0$  as well as competitive, thermally activated, non-radiative de-excitation, from  ${}^5D_0$  to  ${}^7F_6$  through a CTS, and from  ${}^5D_1$  to  ${}^5D_0$  by MPR, or to  ${}^7F_6$  through a CTS. The decay scenario is similar for excitation by other wavelengths, except that for  $488\text{ nm}$  the  ${}^5D_1$  level is excited approximately directly and for  $532\text{ nm}$  there is competitive (and temperature dependent) filling of both  ${}^5D_1$  and  ${}^5D_0$ , either from  ${}^7F_0$  or  ${}^7F_1$ .

Finally, the decay pathway proposed here also provides insight into several so-far unexplained phenomena [20] observed in  $\text{Eu}:\text{7YSZ}$ , a material of interest in luminescence thermometry in thermal barrier coatings. The decay of the  ${}^5D_0$  population in  $\text{YSZ}$  is usually bi-exponential with some variation depending on processing conditions [21], indicating the presence of two kinds of  $\text{Eu}^{3+}$  populations (possibly those associated with an oxygen vacancy and those not). A rise-time has also been observed whose explanation has been uncertain. The time constant of that rise time is similar to the one observed in  $\text{Eu}:\text{Ca}_2\text{Gd}_8\text{Si}_6\text{O}_{26}$  ( $\sim 10\text{ }\mu\text{s}$ , both of which are faster than what has been reported for site-to-site filling [12]; it seems likely, therefore, that the explanation in  $\text{Eu}:\text{YSZ}$  may also be population of  ${}^5D_0$  by  ${}^5D_1$ .

## 5. Conclusions

The useful range of Eu:Ca<sub>2</sub>Gd<sub>8</sub>Si<sub>6</sub>O<sub>26</sub> for decay-time based luminescence thermometry is from room temperature to 800 °C. The intensity is also temperature-sensitive over that range, implying a possible color shift with temperature for white LEDs based in part on Eu:Ca<sub>2</sub>Gd<sub>8</sub>Si<sub>6</sub>O<sub>26</sub> as a possible red phosphor. Excitation using either 532 or 266 nm causes competitive filling of <sup>5</sup>D<sub>1</sub> and <sup>5</sup>D<sub>0</sub> based on direct filling or filling through a CTS, respectively. De-excitation is through radiative decay, filling of <sup>5</sup>D<sub>0</sub> from <sup>5</sup>D<sub>1</sub>, and thermally excited non-radiative decay, primarily through a CTS.

## Acknowledgments

Support for this work has been provided by the NSF Chemical and Transport Systems Division through Grant CTS-0428941.

## Appendix

A rise–fall type decay corresponds to a filling of the emitting level (here, “level 2”) from some higher level (“level 1”) that has its own decay rate. Eq. (3) above accurately reproduces the resultant rise–fall behavior, but the value of  $\tau_{rise}$  is only approximately equal to  $\tau_1$ . The differential equations describing this process are

$$\frac{dN_1}{dt} = -N_1 W_{1,total} \quad (10a)$$

$$\frac{dN_2}{dt} = -N_2 W_{2,total} + N_1 W_{1 \rightarrow 2} \quad (10b)$$

where  $N_i$  is the population of level  $i$  at any time  $t$ ,  $W_{i,total}$  is the total decay rate of level  $i$  as described by Eq. (7) and  $W_{1 \rightarrow 2}$  is the

rate of the process by which level 1 decays to fill level 2. The solution to these equations requires accounting for the initial populations of levels 1 and 2, given here as  $N_1^0$  and  $N_2^0$ :

$$N_2(t) = \left( \frac{N_1^0 W_{1 \rightarrow 2}}{W_{2,total} - W_{1,total}} \exp[-t(W_{1,total} - W_{2,total})] + N_2^0 \right) \times \exp(-tW_{2,total}) \quad (11)$$

This equation is exactly equivalent to Eq. (3) above since  $I$  is directly proportional to  $N_2$ . Thus we see that  $\tau_{rise} \approx \tau_1$  for  $\tau_1 \ll \tau_2$ , which is indeed the case here.

## References

- [1] M.J.J. Lammers, G. Blasse, J. Electrochem. Soc. 134 (1987) 2068.
- [2] T.J. Isaacs, J. Electrochem. Soc. 120 (1973) 654.
- [3] M. Yu, J. Lin, Y.H. Zhou, S.B. Wang, H.J. Zhang, J. Mater. Chem. 12 (2002) 86.
- [4] S.W. Allison, G.T. Gillies, Rev. Sci. Instrum. 68 (1997) 2615.
- [5] S. Kraemer, J. Yang, C.G. Levi, J. Am. Ceram. Soc. 91 (2008) 576.
- [6] M.J. Maloney, US Patent 6,284,323, 2001.
- [7] K. Grant (UCSB), CMAS Degradation of EBCs, Thermal barrier Coatings II, Kloster Irsee, Germany, August 16 2007.
- [8] M.M. Gentleman, J.I. Eldridge, D.M. Zhu, K.S. Murphy, D.R. Clarke, Surf. Coat. Tech. 201 (2006) 3937.
- [9] J.P. Feist, A.L. Heyes, Proc. Inst. Mech. Eng. 214 (2000) 7.
- [10] L. Liu, X. Chen, Nanotechnology 18 (2007) 1.
- [11] G. Blasse, J. Solid State Chem. 14 (1975) 181.
- [12] R.M. Ranson, E. Evangelou, C.B. Thomas, Appl. Phys. Lett. 72 (1998) 2663.
- [13] M.G. Paton, E.N. Maslen, Acta Crystallogr. 19 (1965) 307.
- [14] Y. Masubuchi, M. Higuchi, T. Takeda, S. Kikkawa, Solid State Ionics 177 (2006) 263.
- [15] M.D. Chambers, D.R. Clarke, Surf. Coat. Tech. 202 (2007) 688.
- [16] L.A. Riseberg, H.W. Moos, Phys. Rev. 174 (1968) 429.
- [17] M.T. Berry, P.S. May, H. Xu, J. Phys. Chem. 100 (1996) 9216.
- [18] R. Englman, J. Jortner, J. Mol. Phys. 18 (1970) 145.
- [19] W.H. Fonger, C.W. Struck, J. Chem. Phys. 52 (1970) 6364.
- [20] M.D. Chambers, D.R. Clarke, Surf. Coat. Tech. 201 (2006) 3942.
- [21] V. Kisperksy, M.S. Thesis, University of California, Santa Barbara, 2007.
- [22] M.D. Chambers, P.A. Rousseve, D.R. Clarke, Surf. Coat. Tech. (2008).